Continental Evolution Research Group
University of Adelaide

THE UNIVERSITY OF ADELAIDE
AUSTRALIA

SUB CRUCE LUMEN

Magnetotellurics for onshore petroleum exploration: a case study from the Officer Basin

Clarke Petrick

Supervisor:

Graham Heinson

Honours degree 27th October 2004

MAGNETOTELLURICS FOR ONSHORE PETROLEUM EXPLORATION: A CASE STUDY FROM THE OFFICER BASIN

Clarke Petrick
Continental Evolution Research Group
School of Earth and Environmental Sciences
University of Adelaide
Adelaide SA 5005 Australia
Phone: 0408 859 534
Facsimile: 08 83034347
Clarke.Petrick@student.adelaide.edu.au

Graham Heinson
Continental Evolution Research Group
School of Earth and Environmental Sciences
University of Adelaide
Adelaide SA 5005 Australia
Phone: 08 83035377
Facsimilie: 08 83034347
E-mail: Graham.Heinson@adelaide.edu.au

Left Running Heading: Petrick and Heinson

Right Running Heading: MT Exploration of Officer Basin

Table of Contents

ABSTRACT

The Officer Basin, South Australia, is a sedimentary basin that contains several possible salt diapiric structures that have been partially defined from two-dimensional (2D) seismic transects. This paper reports a case study to assess the potential of using magnetotellurics (MT) and gravity data to delineate salt diapiric structures. The study aimed to develop an economical and low impact technique for greenfields exploration of basins in which hydrocarbon resources may be structurally controlled by salt tectonics. Twenty-six MT sites were deployed across two orthogonal transects (seismic lines 85-0009 and 86-0194), one that crosses a known salt structure and the other with no salt wall structure. For the line 85-0009, the depth to the top of the salt dome was 700 m with a width 2.5 km, and appears to be quite disseminated resulting in low acoustic impedance contrasts. Each 18 km line was two-dimensionally modeled to a depth of 3.5 km and evaluated against the seismically imaged basin model.

We show that the salt diapiric structure is only marginally defined by the MT and gravity data, but with more sites and better quality data the resolution will undoubtedly improve. The salt structure was imaged in the same location as the seismic anomaly, and appears as a slightly more resistive body (>200 Ω.m) compared to the porous sedimentary host (~2-200 Ω.m). The resistivity model imaged the depth of the dipping basement, and is consistent with the gravity data. We conclude that in areas of salt structure poorly imaged by seismic methods, MT may be a significant new exploration tool to delineate potential targets.

Key words: Gravity, Magnetotellurics, Officer Basin, Petroleum Exploration, Salt Diapir.

INTRODUCTION

Petroleum exploration in the Officer Basin began in the 1960s with seismics, aeromagnetics and regional gravity surveys being carried out (Morton and Drexel, 1997). Exploration has been sporadic since then, but over 7000 km of 2D seismic data have now been acquired. Seven petroleum wells and forty-two stratigraphic/deep mineral wells have also been drilled into the Officer Basin, with indication the presence of a deposit. However, to date, no significant oil plays have been discovered. Despite the relatively low levels of exploration in this onshore basin, the petroleum industry in general is yet to make a judgment on the prospectivity of the Officer Basin (Morton, 1996a).

Much of the 2D seismic imaging in the area is of poor quality. Carbonates commonly pose difficulties for seismic reflection surveys because excessive reverberations effectively mask reflections from structures beneath them (Figure 1). Alternative techniques need to be incorporated to reduce the ambiguities in the interpretation of 2D seismic reflection data. The MT experiment presented in this paper was carried out during July-August 2004, and was designed to test the feasibility of MT to delineate the structure of a salt diapirs identified from a 2D seismic survey. The field area is within the eastern Officer Basin, which is located in remote western South Australia (Figure 2).

GEOLOGICAL SETTING

The Officer Basin is Australia's largest present day intracratonic basin (Lindsay and Leven, 1996). The elongate, roughly E-W- trending trough is located in the west of South Australia and extends into Western Australia. The Neoproterozoic to Palaeozoic basin was one of a number of troughs that formerly comprised the Centralian Superbasin (Walter et al., 1995). During the Petermann Orogeny the Centralian Superbasin dismembered into a southern fragment (Officer Basin), and a northern fragment (incorporating the Amadeus, Georgina, Ngalia and Savory Basins) (Haddad et al., 2001; Hoskins and Lemon, 1995; Lindsay and Leven, 1996; Moussavi-Harami and Gravestock, 1995; Walter et al., 1995). The Officer Basin's northern margin is sharply thrust faulted against the exhumed Musgrave Block (Walter and Gorter, 1994). Archaean-Palaeoproterozoic Gawler Craton constrains the basin to the south. The sedimentary sequences found in the Officer Basin were deposited over 500 Ma, from the initial deposition of the Willouran (800 Ma), They comprise shallow-water sediments that were deposited in an extensive sag basin (Preiss and Forbes, 1981; Walter et al., 1992). Three orogenic events then followed, the Petermann Range Orogeny at 550 Ma (Comacho and McDougall, 2000; Lindsay and Leven, 1996); the Delamerian Orogeny 500 Ma (Hand et al., 1999); and finally the Alice Springs Orogeny at 300-400 Ma (Cartwright and Buick, 1999; Hand et al., 1999). The intracratonic thrusting and uplift resulted in the deposition of thick sedimentary sequences, ending in the Carboniferous (Moussavi-Harami and Gravestock, 1995).

A marine shelf-evaporitic sea, depositional setting contributed large volumes of salt into the basin. The intrusion of deep-seated evaporites into overlying sediments may form a

structural or stratigraphic hydrocarbon trap. Commercially important traps are commonly found in sediments associated with rock-salt intrusion (Levorsen, 1967). Salt can have either an active or passive role in its association with petroleum traps. Deformation of sediments enclosing the salt dome is caused by active intrusion of the rising salt mass and subsequent uplifting of adjacent strata (Levorsen, 1967). The source of the salt in the intrusive salt dome is deep-seated, and has developed into salt walls and salt pillows, as shown in Figure 3. Both active and passive salt structures have the potential to form petroleum traps and are actively explored worldwide for this reason (Lerche and O'Brien, 1987).

MAGNETOTELLURIC EXPLORATION

Magnetotelluric methods may be particularly useful in petroleum exploration for situations where the seismic technique fails to image sediment packages beneath rock units that scatter and reflect incident seismic energy (Hoversten et al., 1998). In areas of difficult terrain, such as the Officer Basin MT methods are cheaper and easier to undertake than seismic methods (Cull and Gray, 1989). (Constable et al., 1998; Hoversten et al., 2000) have shown that MT is an increasingly important tool in exploring offshore sedimentary basins. However, little work has been carried out onshore. A similar 1D study was conducted in 1989 over the Eromanga Basin, MT inversions imaged sediment compaction but the results where inconclusive (Cull and Gray, 1989). In the case of the 100,000 km^2 Officer Basin, 2D MT methods may be useful for

determining structural relationships, thickness of sedimentary units and the presence of conductive or resistive masses.

Long-period MT records natural variations of electric and magnetic fields in the band with of 1 to 10^5 s. Such data constrain lithospheric-scale structure (Heinson, 1999; Heinson et al., 1996). However, a marine test above the Gemini structure, Gulf of Mexico, using magnetic sensors with much higher precision, demonstrated that high-quality shallow sea-floor MT data could be acquired, despite the attenuation of naturally occurring fields by electrically conductive seawater (Hoversten et al., 2000). Various model studies have now been carried out to test the feasibility of the MT method to map salt bodies in the Gulf of Mexico (Blood, 2001; Hoversten, 1992; Hoversten et al., 1998; Hoversten and Unsworth, 1994). The resistivity of crystalline salt (>100 Ω.m) is at least ten times greater than surrounding porous sediments (<10 Ω.m), providing a highly suitable target for MT (Constable et al., 1998). Hoversten et al. (2000) showed that with MT data of reasonable quality in the 10^{-3} to 1 Hz (1 to 10^3 s) band, combined with a knowledge of the depth to the top of salt, the base of salt could be mapped.

OFFICER BASIN GEOPHYSICAL EXPLORATION

2D Seismic Lines

Extensive 2D seismic surveys have been conducted in the Officer Basin (Morton and Drexel, 1997). Much of the seismic data produced low-quality images due to the vintage of processing, energy source and high reflectivity contrasts within the sediments,

resulting from the presence of carbonates, crystalline salt (Hoversten et al., 2000). Excessive reverberations within these units mask signals from deeper reflectors (Ogilive and Purnell, 1996). The presence of salt with a density (ρ) of 2.2 kgm^{-2} (Blood, 2001) and a seismic compressional velocity 4500 ms^{-1} (Telford et al., 1998) creates reflection coefficients at its boundary of R=+0.176 in a typical sedimentary profile.

Petty-Ray Geophysical Pty Ltd shot line 85-0009 in 1985 with thumper trucks, to a stacking of 60 fold. Data were then migrated by Hosking Geophysics Corp for Comalco Mineral and Petroleum Exploration. The inferred salt structure runs east-west, perpendicular to the series of north-south seismic lines that intercept it. From the series of 2D seismic transects the width was constrained to be 3.5 km and the length to 12 km. A number of continuous reflectors have been mapped as horizons, further constrained by well logging information. Figure 1 shows an example of the data quality from line 85-0009. The image does not illustrate the typical strong top of salt reflectivity seen in the Gulf of Mexico (O'Brien and Gray, 1996). Instead, the area had been identified due to poor reflections and the upward warping of bedding.

Basement in Figure 1 was identified at 1.2 s TWT in the south and 1.8 TWT in the north, representing a 2° slope to the north. Shallowing of the basin in the south is consistent with trends observed in gravity data (Haddad et al., 2001). Basement depth at the base of the salt dome in about 2.6 km and the interpreted top of salt is at a depth of 700 m. This depth of salt represents maximum dimensions of 2 km in height; a width of 2.5 km and 12 km in length developing a maximum salt affected volume of 20 km^3.

Magnetotellurics

The MT method utilises natural sources of time-varying magnetic fields that induce electric current flow in the Earth. Such fluctuations occur over periods from seconds to hours (Keller and Frischknecht, 1966) The periodicity and polarisation of the inducing field is not predictable, but times of heightened EM signals can be predicted by monitoring of solar flare activity. At low frequencies, natural MT fields consist of periodic variations in Earth's magnetic field. Such variations arise from interactions between particle emissions from the Sun and the Earth's atmosphere and magnetosphere. Magnetic storms, caused by material ejected from flares on the surface of the sun, occur approximately once a month and cause erratic variations in the MT field (Vozoff, 1991). When the flare material enters the Earth's natural magnetic field it induces a current in the earth. The horizontal component of the Earth's magnetic field enhances on the side facing the solar flare cloud due to the Earth's Solar diurnal current (Keller and Frischknecht, 1966). Inducing magnetic events are worldwide, so it is reasonable to treat the MT field at mid-latitudes as a plane-wave source-field.

Computation of the Earth's electrical impedance Z from measurements of orthogonal magnetic (magneto) field B and electric (or telluric) field E yields frequency (period) dependent responses. Time-series data are Fourier transformed to give expressions of apparent resistivity (ρ_a) and phase (ϕ) for each period. These two quantities, measured at a number of locations, are interpreted in terms of the electrical resistivity distribution of the earth as a function of depth. The MT method depends on the penetration of EM energy into the Earth. The MT impedance tensor Z is defined by:

$$\begin{vmatrix} E_x \\ E_y \end{vmatrix} = \begin{vmatrix} Z_{xx} & Z_{xy} \\ Z_{yx} & Z_{yy} \end{vmatrix} \begin{vmatrix} B_x \\ B_y \end{vmatrix} \quad (1)$$

Equation (1) states that B is the inducing field, E the resulting field and Z_{ij} represent the Earth's electrical impedance.

The apparent resistivity, $\rho_{a,}$ of the conductor can be determined from the equation:

$$\rho_a = \frac{1}{\mu\omega}|Z|^2 \quad (2)$$

Phase is defined from the equation:

$$\phi = \arctan(Z) \quad (3)$$

Dimensionality of the Earth

In modelling the sub-surface electrical structure, we must consider how the resistivity varies vertically and laterally. For the trivial case of a homogenous Earth, ρ_a is the same at every frequency, and E leads B in-phase by 45 degrees at all frequencies (Keller and Frischknecht, 1966). In the real non-homogenous case, the phase relation between the two field components varies, and determines the Earth's resistivity distribution (Keller and Frischknecht, 1966). The 1D case depends only on the change in ρ with depth. In 2−D, resistivity varies along one horizontal coordinate across strike and with depth. When resistivity varies with both horizontal coordinates and depth the full 3D structure is displayed (Vozoff, 1991).

For a one-dimensional Earth; $Z_{xx} = Z_{yy} = 0$ and $Z_{xy} = -Z_{yx}$,

$$\mathbf{Z} = \begin{bmatrix} 0 & Z_{xy} \\ -Z_{xy} & 0 \end{bmatrix} \tag{4}$$

Modeling in two dimensions, the x- axis can be mathematically rotated so that it is oriented perpendicular to the strike, allowing the impedance values, $Z_{xx} \neq Z_{yy} \neq Z_{xy} \neq Z_{yx} \neq 0$ to be simplified. Two-dimensional impedance values can be written as $Z_{xx} = Z_{yy} = 0$ and $Z_{xy} \neq Z_{yx} \neq 0$, giving:

$$\mathbf{Z} = \begin{bmatrix} 0 & Z_{xy} \\ Z_{yx} & 0 \end{bmatrix} \tag{5}$$

For a three-dimensional Earth, $Z_{xx} \neq Z_{yy} \neq Z_{xy} \neq Z_{yx} \neq 0$, and thus

$$\mathbf{Z} = \begin{bmatrix} Z_{xx} & Z_{xy} \\ Z_{yx} & Z_{yy} \end{bmatrix} \tag{6}$$

Dimensionality is important because the MT method is sensitive to both structure and electrical resistivity. In a 2D situation, the Transverse Magnetic (TM) mode defines the electric field perpendicular and magnetic field parallel to geological strike. Transverse Electric (TE) mode defines the electric field parallel and the magnetic field perpendicular. These modes are treated independently; TM mode has components E (perpendicular), E (vertical) and B (parallel); TE mode has components E (parallel), B (perpendicular) and B (vertical) (Vozoff, 1972).

FIELD SURVEY

Recent advances in processing and modelling techniques have significantly improved the MT method and its ease of use. The addition of the remote-reference field reduced noise

in magnetic-field measurements (Gamble et al., 1979). Various robust response function estimation methods have increased the accuracy and certainty of data processing (Chave et al., 1987; Egbert, 1997; Egbert and Booker, 1986). Development of 1D, 2D and 3D forward and inverse modelling codes e.g. (Constable et al., 1987; Rodi and Mackie, 2001; Smith and Booker, 1991; Wannamaker et al., 1986) have produced unprecedented modelling capabilities.

In the Officer Basin study, MT data were collected with five instruments. Each instrument comprised a three-component fluxgate magnetometer measuring Bx, By and Bz and an electrode array which measured Ex and Ey components. The north-south and east-west electrodes where reduced in length from 50 m to 10 m. The system configuration is illustrated in Figure 4. This alteration of equipment was performed in the field to reduce the voltage potential difference between electrodes. Due to the heterogeneous nature of the sedimentary basin, self-potential (SP) effects generated large voltage differences, which were off-scale for the recording instrument.

The reduction in dipole length reduced deployment time significantly. Copper sulphate electrolyte-filled pots were used as electrodes and auguring approximately 50 cm into moist sand attained good ground coupling. The on-board computer was set running by a notebook PC with a USB connection to record the signal amplitude at 10 Hz. Each instrument and electrode was buried to a depth of 20 cm below the surface in an attempt to stabilize instrument temperature. However, the arid climate produced daily temperature fluctuations of 30°C. This cyclic variation generated a large electrode offset drift, and in some cases causing voltages to go off-scale. The five instruments were

deployed concurrently to facilitate remote referencing between stations (Gamble et al., 1979).

During each survey, time series of the horizontal electric and magnetic fields were collected simultaneously over five sites. Magnetotelluric responses in the bandwidth of 10-1000s where recorded over 24 hours at each location. The data recorded showed low-levels of signal, due to low-levels of natural time-varying magnetic fields present during the survey period, as noted form the Alice Springs magnetic observatory. A profile of stations was used to image the lateral extent of the body. Two perpendicular lines where selected; 85-0009 (line 85) with a salt structure present and 86-0104 (line 86) without (Figure 4). A site spacing of 1 km was generally used, but some in-filling sites were added, depending on the complexity of structure interpreted from seismic data.

The raw data, initially in binary format, were converted to ASCII files at four-second averages, and MT transfer functions were determined using the RRRMT method by (Chave and Thomson, 1989; Chave et al., 1987). Impedance tensors estimates were calculated for each site over a band width of 10-1000 s. Data was imported into WinGLink program and then modeled using 2-D inversion software (Rodi and Mackie, 2001).

Figure 5 displays MT data as a mode pseudo section for line 85. The pseudo-sections show apparent resistivity in (Ω.m) and phase (in degrees) plotted against period (s) for the TM mode (upper two plots) and TE mode (lower two plots).

In general the resistivity increases from low values at short periods to high values at long periods, The broad increase in apparent resistivity (particularly in the TM mode) in the period band of 10 to 100 s below sites I, J and K shows the measured response from the elevated resistivity of the salt dome. Phase angles are less sensitive to structure and are rather more homogeneous.

Two-dimensional Inversion

The 2D inversion process involves a smooth model inversion routine developed by (Rodi and Mackie, 2001) The routine finds regularized solutions (Tikhonov Regularization) to the 2D-inversion problem for MT data using the method of non-linear conjugate gradients. The forward model simulations are computed using finite-difference equations generated by network analogs to Maxwell's equations. The program inverts for a user-defined 2D mesh of resistivity blocks, extending beyond the dimensions of the survey area.

Two profiles were constructed for lines 85 and 86. Both lines intercept at a common site (A) allowing the lines to be tied see (Figure 4). Not all the MT survey sites were included in the inversion, due to low coherency values and hence large error bars. Thus 14 sites were used for line 85. The north-orientated horizontal electrical channel (E_x) or (TM mode) was input into the inversion algorithm. This channel ran perpendicular to the strike of the salt structure and should record the greatest level of complexity (Wannamaker, 1984). A bandwidth of 0.1-0.0001 Hz (period of 10-1000 s) was selected from the TM mode. A number of smooth MT inversions where run over the 85 line. The starting model in each case was varied between a conductive half space, resistive half space and

seismically constrained models. After 300-600 iterations these models converged to a similar structure. Multiple paths where taken to reach the regional minimum reducing the possibility of the program locating the RMS in a local minimum. Floor-errors were applied to data so an error bar of at least 5% surrounded each point at every frequency to reduce the program over fitting individual points.

The resistivity profile produced from the MT inversion has a causal link with sediment porosity variations with depth (Heinson and Segawa, 1995). The large connected pore spaces of the surface sands reduce in porosity lower in the profile due to increased compaction (Keller and Frischknecht, 1966). Water filled porosity (θ) of sediments can be related to depth of burial (Z) by a simple exponential function,

$$\theta(z) = \theta_0 e^{-az} \tag{7}$$

Combining this equation with Archie's law gives:

$$p = p_w \theta^{-2} \tag{8}$$

$$\rho = p_w (\theta_0 e^{-az})^{-2} \tag{9}$$

The porosity θ_0 of the sediments in generally 50% at the surface, with ground water resistivity of $1\,\Omega$. A value of 1.8 km was used for the constant a^{-1} from (Le Pichon et al., 1990). Figure 6 illustrates the relationship between resistivity and depth that would be expected due to compaction down to the basement. Indicative salt and basement resistivities are also displayed showing the level of contrast with surrounding sediments. Salt has its greatest contrast with sediments at 1 km depth. The sharp change in colour in the MT images at the basement level concurs with offset in the resistivity along the dashed line in Figure 6.

DISCUSSION OF MODELLING RESULTS

Magnetotelluric Results

The Lines 85 and 86 were modeled in all permutations of TM, TE and vertical field (H_z) modes with a consistent model of increasing resistivity down to the dipping basement. From all these, three representative images with low RMS have been presented (Figure 7,8 and 9).

Line 86 was imaged in TM mode in an attempt to depict any structures (Figure 7). No significant anomalies were observed from the data in either pseudo-sections or in the TE modes. Figure 7 shows vertically increasing resistivity, with almost no lateral variation, consistent with a sedimentary profile from an extensional basin (Keller and Frischknecht, 1966). The result from this line accurately represented the horizontal structure of basin along strike with a shallow dip to the west, interpreted from seismic, gravity and basin evolution models (Morton and Drexel, 1997).

Line 85 is of great interest and shows a resistivity deviation from the norm in the TM mode (Figure 8). An increase in resistivity below stations I J and K is coincident with inferred salt from seismic imaging. Presence of this feature is not as clear in the TE mode (Figure 9), as the structure is orientated parallel to the electric dipole in this mode, and there would be little electric field change along strike (Wannamaker, 1984). However, the basement structure (> 1000 Ω.m), which is laterally extensive, has been

well modelled in both modes. Interestingly a slight rise in the basement below site M coincides with a salt withdrawal zone interpreted by (Lindsay and Leven, 1996).

A limitation of MT modelling is that it represents resistivity as an averaging of the earth's true resistivity, reducing the definition of any structure observed. Modelling also works on a smoothing factor, further reducing anomalous features and fitting them to a simpler model. The contrast between porous saturated sediments (1-20 Ω.m) and salt (100 Ω.m) provides an order of magnitude contrast, but this can be overwhelmed by difference of two orders of magnitude between the sediments and basement (1000 Ω.m) which is much more prominent.

The non-uniqueness of MT provides a high level of variability and allows a number of possible geological interpretations. Additional information can quickly constrain the model. Seismic distortion is indicative of a salt presence. The presence at depth of the the evaporite Alinya Formation (Figure 1) provides a source of salt to explain the resistive anomaly. The salt structure could be a salt wall, or a salt migration.

The salt wall hypothesis was tested using a seismically defined forward model. The basement architecture was maintained from Figures 8 and 9 which were already consistent with seismic data. A pillar of resistivity 100 Ω.m was drawn in to represent a salt dome. The model was run for 100 iterations in the TM mode. The smoothing factor was reduced for the inversions so as to maintain as much structure as possible. The salt structure presence was maintained after 100 iterations and little variation was seen in the basement (Figure 10). The RMS (1.277) recorded was slightly lower than in Figures 8

and 9, which was recorded from the unconstrained model. The resistivity high on the basement is reduced in Figure 8, and the resistivity in the zone of salt dome is increased. This is due the non-uniqueness of MT and the number of local minimums. The result is an accurate model consistent with the seismic salt wall interpretation produced by PIRSA (2000).

As a test of model sensitivity, a second identical salt structure was placed under site G in Figure 11. The structure was inconsistent with existing seismic data to test the sensitivity of the model to this structure, under the same conditions as in the previous salt dome forward model (Figure 10). Figure 11 illustrates the model after 100 iterations. We note that the second salt dome is not preserved in the inversion, and is therefore not required by the TM mode data. The lower figure indicates model sensitivity, with blue regions showing maximum sensitivity and red low sensitivity. There is good sensitivity directly beneath sites I, J and K indicating that we have confidence that the salt wall is required part of the model.

The region of salt was not as clearly imaged as for other salt bodies in the Gulf of Mexico (Constable et al., 1998). We suggest that the the salt is widely disseminated. This would explain the low level of resistive contrast and the absence of a strong reflection from the top of the salt structure.

An interpretation of Figure 7 was conducted independent of existing basin knowledge. A salt roller model can be used to explaine the resistivity result, because salt migrates, it forms laterally extensive salt bands (Guglielmo et al., 1997). This is the simplest

explanation and would be the case if MT were the sole exploration tool. It can be seen from seismic that the edges of the affected area are vertical and the displacement of reflector is greater than that of the salt roller accumulation. The salt structure does not display the lateral branching or relay patterns of the seismic roller model (Guglielmo et al., 1997).

Gravity Results

The gravity profile along line 85 was taken at 500 m intervals with a La Coste Romberg Gravimeter (Figure 4). Bouguer gravity anomalys were calculated accounting for a free air corrections, instrumental drift and Bouguer slab. It must be noted that due to the trial nature of the survey, latitude corrections and terrain were not performed. Elevations were inferred from seismic shot point locations to an accuracy of 1 m (Figure 12). Sand dunes over the survey line had been mobile since they were first recorded in 1985. Due to this fact and the interpolation of elevation between seismic recordings, errors were increased to 2.5 m. This uncertainty was included into free air and Bouguer corrections and represent an underlying 0.5 mGal uncertainty.

A 20 mGal slope across the profile was delineated confirming the increased basement depth to the north and the filing of younger sediments of lower density (Haddad et al., 2001). The dipping basin and sedimentary profile was modelled to a depth of 10 km (Figure 12). A small -3 mGal gravity anomaly at site K (location E788386 N6868774) overlies the salt body. Modelling of gravity profile in Model Vision 5.0 shows that the body can be represented as a body of slightly lower density putting further constraint on

the overall interpretation. However due to the accuracy of gravity data, further inferences were not possible.

Imaging of comparative densities between pure salt and surrounding sediment can be constrained in modelling by assigning known values of salt. Crystalline salt has a density 2.2 g/cm^3 that remains constant under increasing pressure, unlike sediments which increases as a function of depth due to compaction. An estimation of concentration is needed in the contaminated-salt block case. Assuming 80% salt at 2.2 g/cm^3 and 20% anhydrite at 2.90 g/cm^3 a density of 2.34 g/cm^3 is produced. This ratio has been successful in gravity modelling in the South Oman basin (Blood, 2001). The volume and depth of salt can be calculated from gravity modelling, but density values of the surrounding sediments must be constrained (Smith & Whitehead, 1989). This can be calculated from base line gravity response, using density wireline log well data or estimations of compaction rates. Regional variations in geology make the identification of small negative amplitude anomalies extremely difficult; a feature also reported by Smith and Whitehead (1989). Closely spaced gravity measurements have, however, identified basement and, indicate the possible presence of salt. The size of the salt dome has made identification difficult. It has been stated that a salt body of dimensions greater than 5 km is needed amongst compacted sediments to be resolved independently by gravity (Blood, 2001).

CONCLUSION

MT has proven itself as a significant geophysical technique for the onshore investigation of subsurface salt structure in sedimentary basins. Resistivity model studies have independently imaged 1000 Ω.m resistive basement over two profiles at a depth of 2.5 km. Sedimentary sequence resistivities were shown to increase down the profile. Calculations of porosity variation with depth produced matching resistivities. Identification of elevated resistivities were depicted, and are associated with salt bodies. With the addition of seismic data MT modelling allowed the resistivity and dimensions to be further constrained to 100 Ω.m to a depth of 700 m and a width of 2.5 km. The seismically-constrained salt wall interpretation was confirmed with a reduction in misfit.

The MT method is a cheap and effective approach for mapping salt onshore. Minimal environmental impact, remote access and low logistical requirements are all characteristics that make MT a unique deep exploration technique for areas that have poor seismic coverage. Development of sites over existing seismic profiles allows higher confidence in interpretation. Quality of data could be significantly enhanced with additional instruments, closer spaced deployments and an increase in recording time.

ACKNOWLEDGEMENTS

Special thanks go to my supervisor, Dr Graham Heinson for dedicating his time and knowledge to this endeavour. I would like to thank Dr Peter Boult and PIRSA for developing and financially supporting this project. Gratitude also goes to the ASEG Research Foundation for their financial assistance. Adam Davey, Oliver Ninglegen,

Dennis Rippe and Stephan Thiel were essential participants during expeditions to the Officer Basin. We wish to thank the Maralinga Tjarutja for permitting access to their land.

REFERENCES

Blood, M. F., 2001, Exploration for a frontier salt basin in Southwest Oman: *The Leading Edge*, **20**, 1252.

Carter, N. L. and Hanansen, F. D., 1983, Creep of rock salt: *Tectonophysics*, **116**, 275-333.

Cartwright, I. and Buick, I. S., 1999, The flow of surface derived fluids through Alice Springs age middle-crustal ductile shear zones, Reynolds Range, central Australia: *Journal of Metamorphic Geology*, **17**, 397-414.

Chave, A. D. and Thomson, D. J., 1989, Some comments on magnetotelluric response function estimation: *Journal of Geophysical Research*, **94**, 14215-14225.

Chave, A. D., Thomson, D. J. and Ander, M. E., 1987, On the robust estimation of power spectra, coherences, and transfer functions: *Journal of Geophysical Research*, **92**, 633-648.

Comacho, A. and McDougall, I., 2000, Intracratonic strike-slip partitoned transpression and the formation and exhumation of eclogite facies rocks: an example from the Musgrave Block, central Australia: *Tectonics*, **19**, 978-996.

Constable, S. C., Orange, A. S., Hoversten, G. M. and Morrison, H. F., 1998, Marine magnetotellurics for petroleum exploration Part I: A sea-floor equipment system: *Geophysics*, **63**, 816-825.

Cull, J. P. and Gray, J. D., 1989, Sedimentary Compaction and Magnetotelluric Data in the Eromanga Basin: *Exploration Geophysics*, **20**, 335-337.

Egbert, G. D., 1997, Robust multiple-station magnetoturic data processing: *Geophysics Journal of the royal Astronomical Society* , **130**, 475-496.

Egbert, G. D. and Booker, J. R., 1986, Robust estimation of geomagnetic transfer functions: *Geophysics*, **87**, 173-194.

Gamble, T. D., Goubau, W. M. and Clarke, J., 1979, Magnetotellurics with remote magnetic reference: *Geophysics*, **44**, 53-68.

Guglielmo, G., Jackson, J. M. P. A. and Vendeville, B. C., 1997, Three-dimensional visualization of salt walls and associated fault systems: *AAPG Bulletin*, **81**, 46-61.

Haddad, D., Watts, A. B. and Lindsay, J., 2001, Evolution of the intracratonic Officer Basin, central Australia: implications from subsidence analysis and gravity modelling: *Basin Research*, **13**, (217-238).

Hand, M., Mawby, J., Kinny, P. and Foden, J., 1999, U-Pb ages from the Hart's Range, central Australia: evidence for early Ordovician extention and constraints on Carboniferous metamorphism: *Journal of Geological Society, London*, **156**, 715-730.

Heinson, G. and Segawa, J., 1995, Electrokinetic signature of the Nankai Trough accretionary complex: preliminary modelling for the Kaiko-Tokai program: *Physics of the Earth and Planetary Interiors*, **99**, 33-53.

Hoskins, D. and Lemon, N., 1995, Tectonic development of the eastern Officer Basin, central Australia: *Exploration Geophysics*, **26**, 243-246.

Hoversten, G. M., 1992, Seaborne electromagnetic subsalt exploration: *EOS*, **73**, 313.

Hoversten, G. M., Morrison, H. F. and Constable, S. C., 1998, Marine magnetotellurics for petroleum exploration, Part II: Numerical analysis of subsalt resolution: *Geophysics*, **63**, 826-840.

Hoversten, M. G., Constable, S. C. and H., M. F., 2000, Marine magnetotellurics for base-of-salt mapping: Gulf of Mexico field test at the Gemini structure: *Geophysics*, **65**, 1476-1488.

Keller, G. V. and Frischknecht, F. C., 1966, Electrical Methods in Geophysical Prospecting, *Pergamon Press, Inc.*

Le Pichon, X., Henry, P. and Lallemant, S., 1990, Water flow in the Barbados Accretionary Complex: *Geophysical Research*, **95**, 8945-8967.

Lindsay, J. F. and Leven, J. H., 1996, Evolution of a Neoproterozoic to Palaeozoic intracratonic setting, Officer Basin South Australia: *Basin Research*, **8**, 403-424.

Levorsen, A.I., 1967, Geology of Petroleum, 2nd Edition. publisher, Freeman, W.H. & Co.

Lerche, I. and O'Brien, J. J., 1987, Dynamic geology of salt and related structures, published *Academic Press, Inc.*

Morton, J. G. G., 1996, MESA Petroleum industry survey: *South Australian. Department of Mines and Energy report book*, **96**, 17-63.

Morton, J. G. G. and Drexel J. F, 1997, The Petroleum Geology Of South Australia, Volume 3: Officer Basin, 1-321.

Moussavi-Harami, R. and Gravestock, D. I., 1995, Burial history of the eastern Officer Basin, South Australia: *AAPG Journal*, **35**, 307-320.

O'Brien, M. J. and Gray, S. H., 1996, Can we image beneath salt?: *The Leading Edge*, **15**,

Ogilive, J. S. and Purnell, G. W., 1996, Effects of salt-related mode conversion on subsalt prospecting: *Geophysics*, **61**, 331-348.

Preiss, W. V. and Forbes, B. G., 1981, Stratigraphy, correlaion and sedimentary history of Adeladiean (Late Proterozoic) basins in Australia: *Precambrian Research*, **15**, 255-304.

PIRSA, 2002, Officer Basin, *Primary Industries and Resourses South Australia*, 1-13.

Rodi, W. and Mackie, R. L., 2001, Nonlinear conjugate gradients algorithm for 2-D magnetotelluric inversion: *Geophysics*, **66**, 174-187.

Smith, J. T. and Booker, J. R., 1991, Rapid inversion of two and three-dimensional magnetotelluric data: *Journal of Geophysical Research*, **96**, 3905-3922.

Vozoff, K., 1972, The magnetotelluric method in exploration of sedimentary basins: *Geophysics*, **37**, 98-141.

Vozoff, K., 1991, The magnetotelluric method, in Nabighian, M. N., Ed., Glectromagnetic methods in applied geophysics, 2: *Society of Exploration Geophysists*, 641-711.

Walter, M. R., Veevers, J. L., Calver, C. R., Grey, K. and Hilyard, D., 1992, The Proterozoic Centralian Superbasin: a frountier petroleum province: *Bulletin American Association of Perroleum Geology*, **76**, 1132.

Walter, M. R., Veevers, J. L., Calver, C. R. and Grey, K., 1995, Neoproterozoic stratigraphy of the Centralian Superbasin, Australia.: *Precambrian Research*, **73**, 173-195.

Walter, M. R. and Gorter, J. D., 1994, The Neoproterozoic Centralian Superbasin in Western Australia. *Petroleum Exploration Society Australia*, 851-964.

Wannamaker, P. E., Stodt, J. A. and Rijo, L., 1986, A stable finite element solution for two-dimensional modeling: *Geophysics*, **37**, 277-296.

Smith, J. T. and Booker, J. R., 1991, Rapid inversion of two and three-dimensional

magnetotelluric data: *Journal of Geophysical Research*, **96**, 3905-3922.

Telford, W. M., Geldart, L.P. and Sheriff, R. E, 1998, Applied Geophysics Second edition, *Cambridge University Press.*

Vozoff, K., 1972, The magnetotelluric method in exploration of sedimentary basins: *Geophysics*, **37**, 98-141.

Vozoff, K., 1991, The magnetotelluric method, in Nabighian, M. N., Ed., Electromagnetic methods in applied geophysics, 2: *Society of Exploration Geophysists*, 641-711.

Walter, M. R., Veevers, J. L., Calver, C. R. and Grey, K., 1995, Neoproterozoic stratigraphy of the Centralian Superbasin, Australia.: *Precambrian Resurch*, **73**, 173-195.

Walter, M. R., Veevers, J. L., Calver, C. R., Grey, K. and Hilyard, D., 1992, The Proterozoic Centralian Superbasin: a frountier petroleum province: *Bulliten American Association of Perroleum Geology*, **76**, 1132.

Wannamaker, P. E., Stodt, J. A. and Rijo, L., 1986, A stable finite element solution for two-dimensional modeling: *Geophysics*, **37**, 277-296.

Yilmas, O., 2001, Seismic data analysis. Processing, inversion and interpretation of seismic data: *SEG Investigation in Geophysics*, **10**, 171-213.

TABLES AND FIGURE CAPTIONS

Table 1: MT data recorded in the Officer Basin in July and August 2004. Lines 85 and 86 are aligned north-south and east-west respectively. Site A is the intercept location and is common to both lines.

Table 2: Gravity data locations and Bouguer gravity calculations. Readings were taken at approximately 500 m intervals away from topographic highs as to reduce the need for terrain corrections.

Fig. 1: Reflection seismic data recorded in 1985, a number of horizons have been traced. The salt dome in question has been outlined in yellow. Adapted from Morton (1997).

Fig. 2: The map of the Officer Basin shows general geology within South Australia. The darkened square in the center map shows the location of the study area and the orientation of profiles. Munta 1 well is located on the western end of line 86. Basin depth increases towards the Manyari Trough. Adapted from PIRSA, (2002).

Fig. 3: Schematic cross section of the Officer Basin. The diapric wall is located between wells Karlaya 1 and Munta 1 is a close representation of seismic line 85. Adapter from PIRSA, (2002).

Fig. 4: Illustrates the site locations of MT and gravity lines with respect to the salt wall. Site A is common to both lines and Munta 1 is located at site O on line 86. The MT array shows the instrument deployment.

Fig. 5: Line 85 pseudo-sections. The TM mode represents a broad resistive high over the area of the salt dome. TE mode also displays this anomaly at the surface with an additional zone of high resistivities at high periods.

Fig. 6: The basin resistivity graph generated from equation (9) shows the change in resistivity with depth in the sedimentary profile. The dark solid line represents the higher more homogeneous resistivity of the basement. Triple lines displayed the salt and the variation of the resistivity contrast with the sediments.

Fig. 7: Line 86 is located along the flank of the salt dome at a distance of 7 km. The MT model shows the vertical profile and accurately depicts westerly dip in the basement. The image has been overlaid with reflection seismic data and mapped horizons have been interpreted from well Munta 1.

Fig. 8: Line 85 crosses the salt dome at locations I, J and K. The MT image shows a slight resistivity high in the TM mode, along with the basin profile and basement. Below site B is increased resistively associated with a salt withdrawn zone.

Fig. 9: Line 85 was imaged in the TE mode, the same high resistivity bump was not shown as in Figure 8 but a slight elevation in resistivity at 1 km depth can be observed. The basement structure was close to that of the TM mode.

Fig. 10: This MT image is the result of 100 iterations of a seismically defined TM forward mode. The number iterations and a reduction in RMS from Figure 8 gives the reader confidence in the image. MT has imaged the salt dome extremely close to that seen in Figure 1.

Fig. 11: Line 85 MT image in TM mode. A reproduction of Figure 10 was carried out with 2 identical domes, to test the discriminative characteristics of the inversion process. The result shows a reduction in dome 2 and an increase in RMS error. The sensitivity of the program with depth shows that both domes are in equivalent zones. The second dome has been reduces as it doesn't fit the data.

Fig. 12: Graph of Bouguer gravity at each site location. The lower figure shows 1985 seismic shot point elevations used in gravity calculations. It can be seen that the instrument elevation has been correctly calculated, as there no correlation between graphs.

Fig. 13: The gravity model shows dipping basement consistent with the MT figures and shows a small -3 mGal anomaly above the salt dome.

EQUATIONS

$$\begin{vmatrix} E_x \\ E_y \end{vmatrix} = \begin{vmatrix} Z_{xx} & Z_{xy} \\ Z_{yx} & Z_{yy} \end{vmatrix} \begin{vmatrix} B_x \\ B_y \end{vmatrix} \quad (1)$$

$$\rho_a = \frac{1}{\mu\omega}|Z|^2 \quad (2)$$

$$\phi = \arctan(Z) \quad (3)$$

$$\mathbf{Z} = \begin{bmatrix} 0 & \mathrm{Z_{xy}} \\ -\mathrm{Z_{xy}} & 0 \end{bmatrix} \quad (4)$$

.

$$\mathbf{Z} = \begin{bmatrix} 0 & \mathrm{Z_{xy}} \\ \mathrm{Z_{yx}} & 0 \end{bmatrix} \quad (5)$$

$$\mathbf{Z} = \begin{bmatrix} \mathrm{Z_{xx}} & \mathrm{Z_{xy}} \\ \mathrm{Z_{yx}} & \mathrm{Z_{yy}} \end{bmatrix} \quad (6)$$

$$\theta(z) = \theta_0 e^{-az} \quad (7)$$

$$p = p_w \theta^{-2} \quad (8)$$

$$\rho = p_w(\theta_0 e^{-az})^{-2} \quad (9)$$

Officer Basin Magnetotelluric Site Locations

Site	Field Lable	Instrument	Latitude	Longitude	Easting	Northing	Elevation	GDA 84 Zone
			Line 85-0009					
A	8500	5	-28 21.7284	131 56.3346	788059	6859169	312	52
B	8501	4	-28 21.2994	131 56.2680	787970	6859964	319	52
C	8502B	3	-28 20.6778	131 56.3016	788048	6860943	310	52
D	8503	2	-28 20.3916	131 56.3004	788055	6861640	319	52
E	8504	1	-28 20.0892	131 56.3004	788077	6862199	318	52
F	8517	5	-2819.5042	13156.4408	788444	6863273	327	52
G	8506	1	-2818.7116	13156.4282	788348	6864739	328	52
H	8507	3	-2818.1584	13156.4288	788374	6865761	330	52
I	8509	5	-2817.0844	13156.3868	788353	6867748	316	52
J	8516	1	-2816.8120	13156.3814	788357	6868251	321	52
K	8510	5	-2816.5288	13156.3916	788386	6868774	323	52
L	8513	4	-2814.9154	13156.3202	788342	6871758	342	52
M	8514	4	-2814.0670	13156.2896	788330	6873327	366	52
N	8515	3	-2813.2906	13156.2806	788350	6874761	361	52
			Line 86-0194					
O	8605	1	-28 21.6450	131 53.5806	783562	6859432	343	52
P	8602	4	-28 21.6846	131 55.1136	786065	6859298	333	52
Q	8501	4	-28 21.2994	131 56.2680	787970	6859964	319	52
A	8500	5	-28 21.7284	131 56.3346	788059	6859169	312	52
R	8606	1	-28 21.6996	131 56.9520	789069	6859198	304	52
S	8607	3	-28 21.2700	131 57.3450	789731	6859976	307	52
T	8608	4	-28 21.2670	131 57.9708	790754	6859956	293	52
U	8609	5	-28 21.2616	131 58.5864	791761	6859941	284	52
V	8610	1	-28 21.0516	131 59.1750	792732	6860305	285	52
W	8613	5	-28 20.9244	132 00.9414	207452	6860545	326	53
X	8614	1	-28 21.0402	132 01.5438	208442	6860355	325	53
Y	8615	2	-28 21.1998	132 02.1270	209403	6860084	334	53
Z	8616	5	-28 21.2988	132 02.7294	210392	6859925	322	53

Gravity Locations & Calculations

Station	Easting	Northing	Time in minutes	Gravity (Counts)	Time since start in min	Earth tide correction	Grav(obs)-ETC	Cal(G)	seismic	Free air Correction	Bougau correction	G(BA) =CalG+FAC-BC
F1	788431	6863277	8:03:32	27335.5	0.00	0.0000	2733.55	2815.6	334	103.0	30.8	2887.8
F1rpt	788435	6863279	12:25:08	27339.0	261.60	0.3500	2733.55	2815.6	334	103.0	30.8	2887.8
2	788252	6863849	8:13:24	27308.5	9.87	0.0132	2730.84	2812.8	335	103.3	30.9	2885.2
3	788269	6864362	8:21:30	27310.0	17.97	0.0240	2730.98	2812.9	334	103.0	30.8	2885.2
4	788292	6864888	8:28:15	27290.0	24.72	0.0331	2728.97	2810.8	337	104.0	31.1	2883.7
5	788307	6865392	8:34:48	27286.0	31.27	0.0418	2728.56	2810.4	337	104.0	31.1	2883.3
6	788330	6865977	8:43:05	27269.0	39.55	0.0529	2726.85	2808.7	340	104.9	31.3	2882.2
7	788356	6866512	8:48:41	27272.0	45.15	0.0604	2727.14	2809.0	334	103.0	30.8	2881.2
8	788369	6867019	8:54:56	27291.0	51.40	0.0688	2729.03	2810.9	326	100.6	30.1	2881.4
9	788387	6867519	9:02:36	27289.0	59.07	0.0790	2728.82	2810.7	325	100.3	30.0	2881.0
10	788413	6868054	9:09:24	27277.0	65.87	0.0881	2727.61	2809.4	326	100.6	30.1	2880.0
10rpt	788414	6868054	12:05:11	27276.5	241.65	0.3233	2727.33	2809.1	326	100.6	30.1	2879.7
11	788429	6868561	9:15:42	27255.5	72.17	0.0966	2725.45	2807.2	329	101.5	30.3	2878.4
12	788468	6869100	9:46:05	27226.0	102.55	0.1372	2722.46	2804.1	331	102.1	30.5	2875.7
13	788486	6869632	9:51:35	27205.5	108.05	0.1446	2720.41	2802.0	335	103.3	30.9	2874.5
14	788503	6870225	9:57:56	27202.0	114.40	0.1531	2720.05	2801.6	333	102.7	30.7	2873.7
15	788533	6870836	10:02:58	27174.0	119.43	0.1598	2717.24	2798.8	339	104.6	31.2	2872.1
16	788554	6871408	10:07:54	27140.5	124.37	0.1664	2713.88	2795.3	346	106.7	31.9	2870.1
17	788574	6871923	10:13:44	27098.5	130.20	0.1742	2709.68	2791.0	356	109.8	32.8	2868.0
18	788594	6872434	10:18:27	27074.0	134.92	0.1805	2707.22	2788.4	364	112.3	33.6	2867.2
19	788609	6872954	10:24:50	27027.5	141.30	0.1890	2702.56	2783.6	378	116.6	34.8	2865.4
19rpt	788605	6872952	11:47:02	27027.0	223.50	0.2990	2702.4	2783.5	378	116.6	34.8	2865.2
20	788623	6873459	10:30:01	27040.0	146.48	0.1960	2703.8	2784.9	367	113.2	33.8	2864.3
21	788642	6873969	10:39:20	27030.5	155.80	0.2084	2702.84	2783.9	365	112.6	33.6	2862.9
N22	788657	6874438	10:46:12	27014.0	162.67	0.2176	2701.18	2782.2	368	113.5	33.9	2861.8
	Drift Gravity Counts per minute				**0.013**							

Locations are recorded in GDA 84 in Zone 52

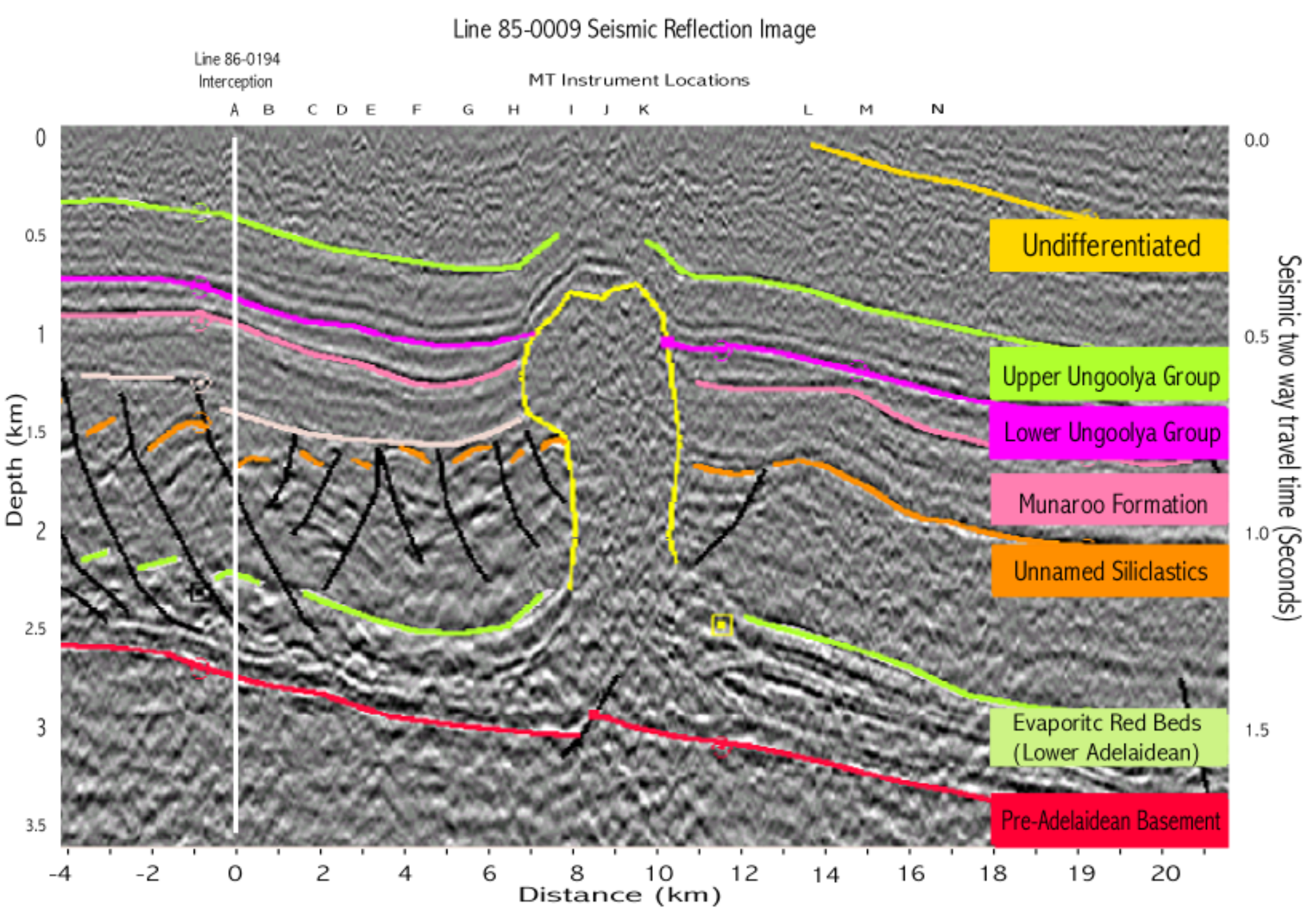
Line 85-0009 Seismic Reflection Image
Line 86-0194
Interception
MT Instrument Locations
A B C D E F G H I J K L M N
0
0.5
1
1.5
2
2.5
3
3.5
Depth (km)
0.0
0.5
1.0
1.5
Seismic two way travel time (Seconds)
Undifferentiated
Upper Ungoolya Group
Lower Ungoolya Group
Munaroo Formation
Unnamed Siliclastics
Evaporitc Red Beds
(Lower Adelaidean)
Pre-Adelaidean Basement
-4 -2 0 2 4 6 8 10 12 14 16 18 19 20
Distance (km)

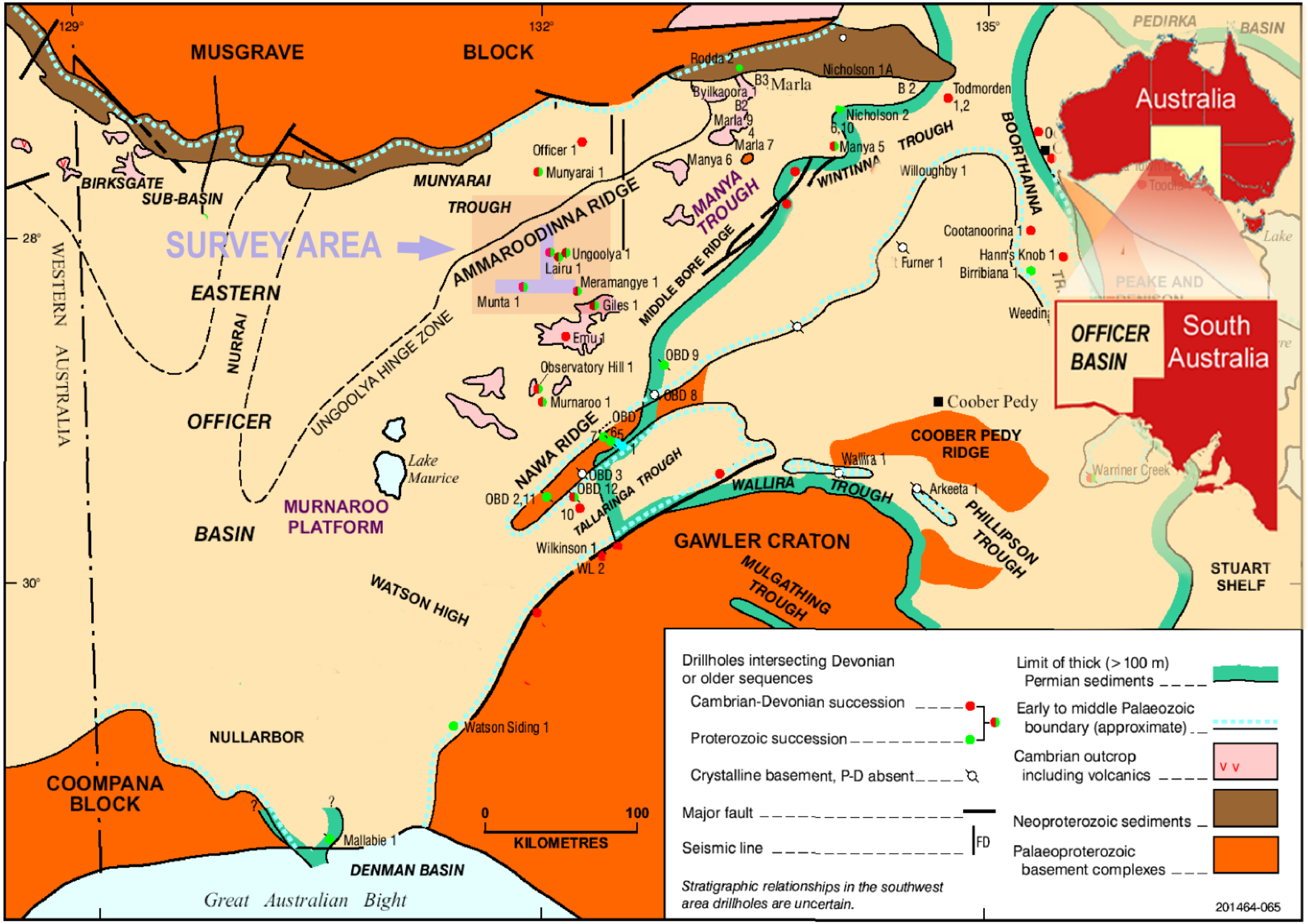
MUSGRAVE BLOCK
BIRKSGATE SUB-BASIN
WESTERN AUSTRALIA
EASTERN
NURRAI
OFFICER
BASIN
MUNYARAI TROUGH
SURVEY AREA
AMMAROODINNA RIDGE
UNGOOLYA HINGE ZONE
MANYA TROUGH
MIDDLE BORE RIDGE
WINTINNA TROUGH
BOORTHANNA TROUGH
NAWA RIDGE
TALLARINGA TROUGH
WALLIRA TROUGH
COOBER PEDY RIDGE
PHILLIPSON TROUGH
MULGATHING TROUGH
MURNAROO PLATFORM
WATSON HIGH
GAWLER CRATON
STUART SHELF
NULLARBOR
COOMPANA BLOCK
DENMAN BASIN
Great Australian Bight
Lake Maurice
PEDIRKA BASIN
Australia
OFFICER BASIN
South Australia
PEAKE AND
Rodda 2
Nicholson 1A
Byilkaoora 1
B3 Marla
B 2
Marla 9
Marla 7
Nicholson 2
Todmorden 1,2
Manya 5
Manya 6
Willoughby 1
Officer 1
Munyarai 1
Ungoolya 1
Lairu 1
Meramangye 1
Munta 1
Giles 1
Emu 1
Observatory Hill 1
Murnaroo 1
OBD 9
OBD 8
OBD 7
OBD 3
OBD 12
OBD 2,11
10
Wilkinson 1
WL 2
Watson Siding 1
Mallabie 1
Furner 1
Cootanoorina 1
Hann's Knob 1
Birribiana 1
Weedina
Coober Pedy
Wallira 1
Arkeeta 1
Warriner Creek
Lake
129°
132°
135°
28°
30°
0
100
KILOMETRES
Drillholes intersecting Devonian or older sequences
Cambrian-Devonian succession
Proterozoic succession
Crystalline basement, P-D absent
Major fault
Seismic line
FD
Stratigraphic relationships in the southwest area drillholes are uncertain.
Limit of thick (>100 m) Permian sediments
Early to middle Palaeozoic boundary (approximate)
Cambrian outcrop including volcanics
Neoproterozoic sediments
Palaeoproterozoic basement complexes
201464-065

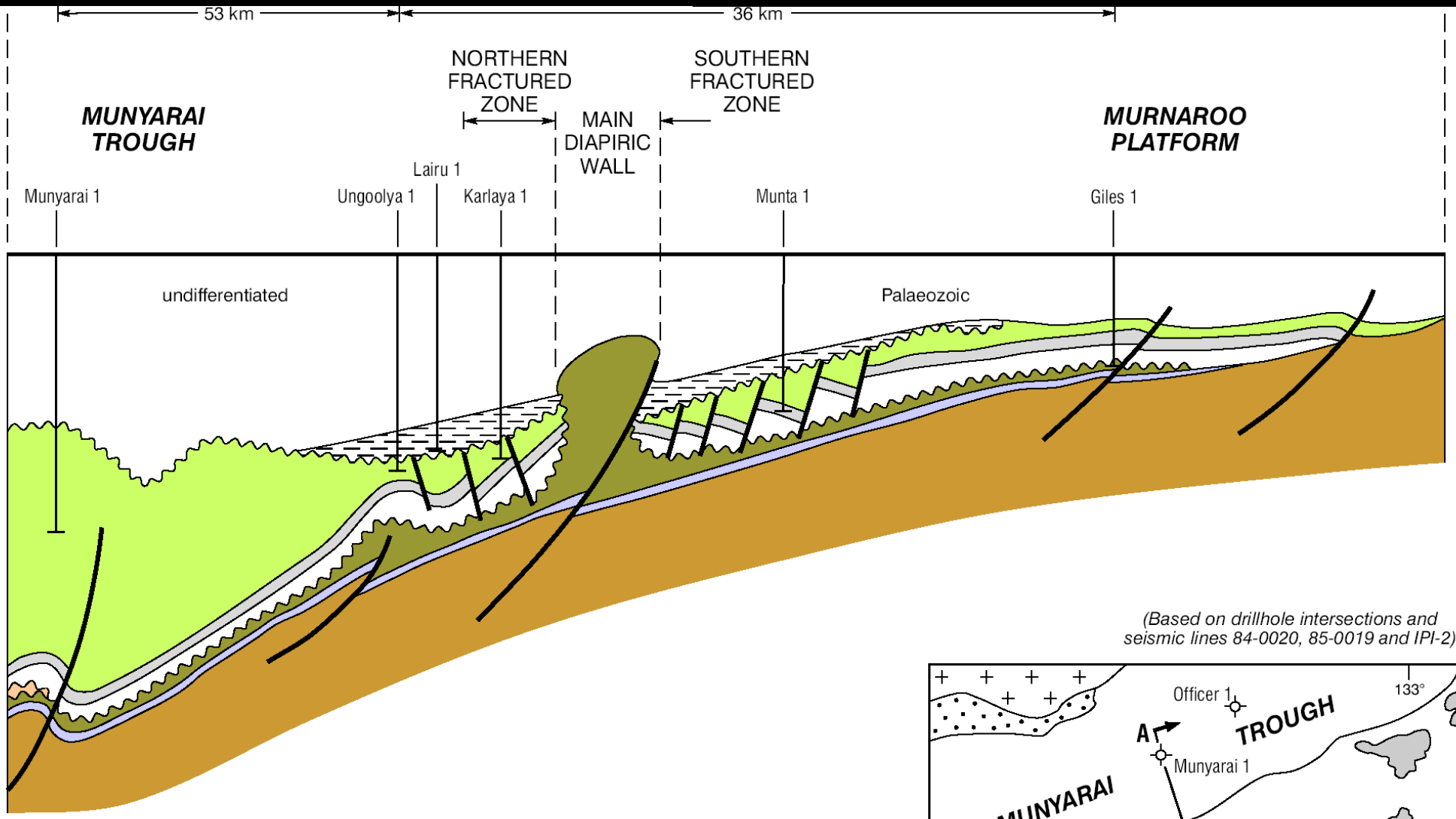

(Based on drillhole intersections and seismic lines 84-0020, 85-0019 and IPI-2)

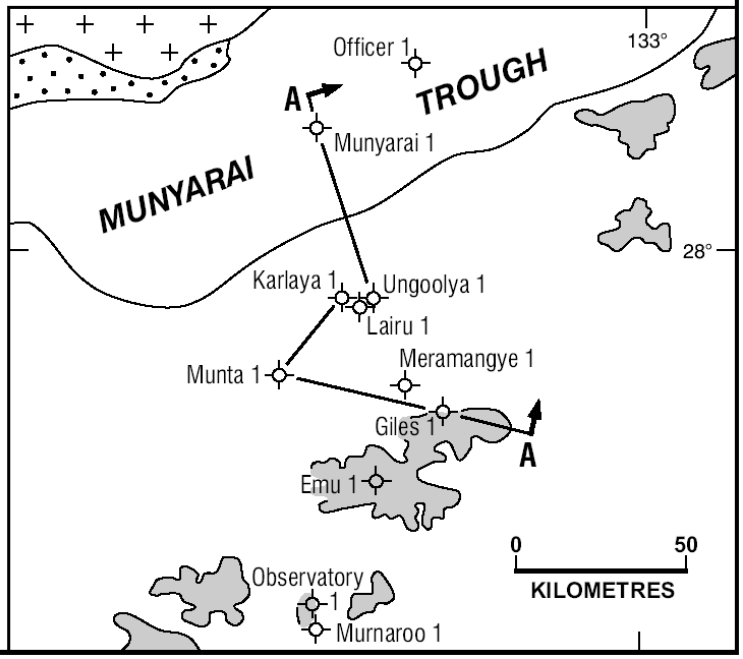

Upper Ungoolya Group

Lower Ungoolya Group

Murnaroo Formation

Unnamed siliciclastics (Upper Adelaidean)

Pindyin Sandstone

Unnamed evaporitc red beds (Lower Adelaidean)

Seismically identified unit

Pre-Adelaidean basement

Seismically identified unconformity

Fault

97-0302 MESA

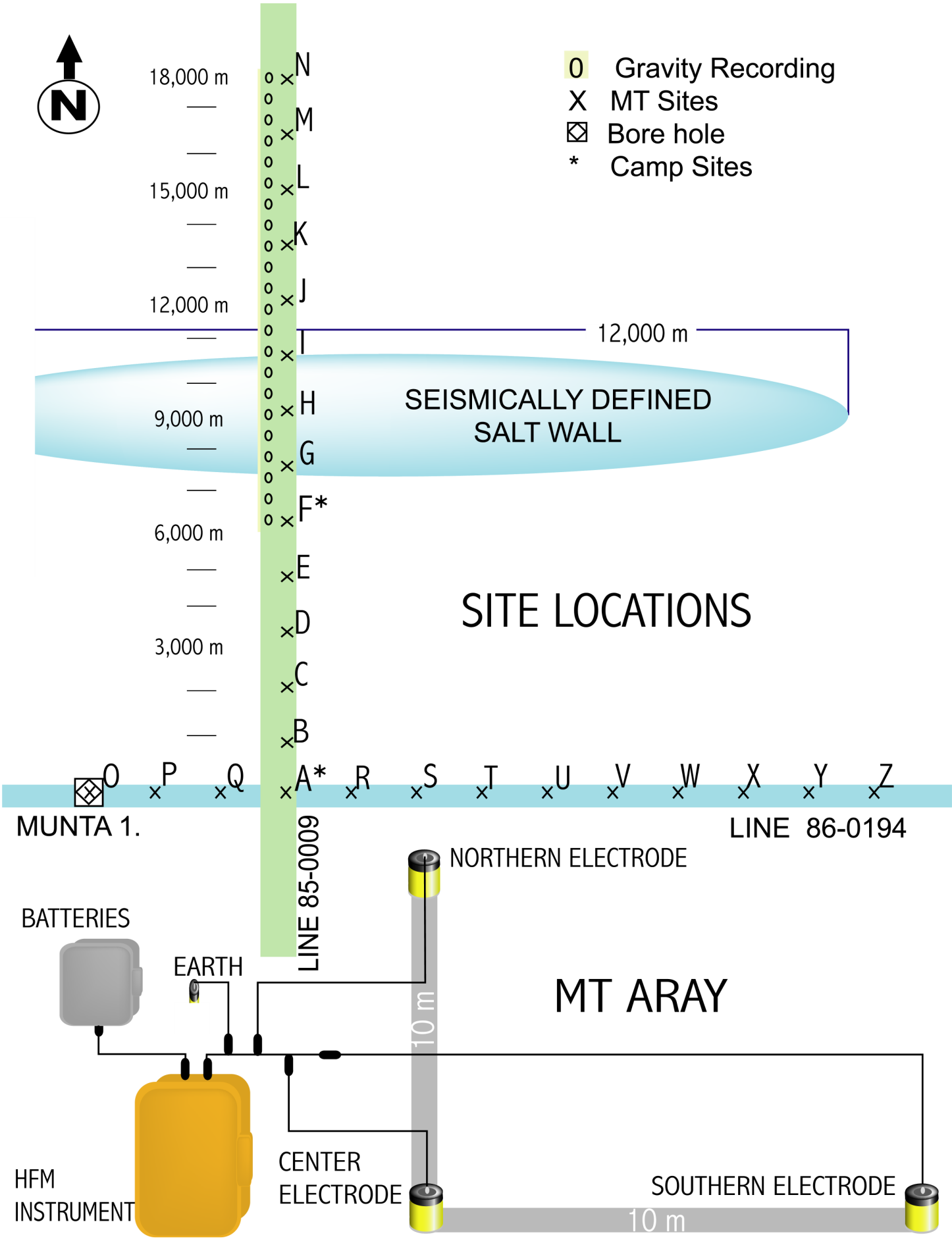
N
18,000 m
15,000 m
12,000 m
9,000 m
6,000 m
3,000 m
0 Gravity Recording
X MT Sites
Bore hole
* Camp Sites
N
M
L
K
J
I
H
G
F*
E
D
C
B
A*
O
P
Q
R
S
T
U
V
W
X
Y
Z
12,000 m
SEISMICALLY DEFINED
SALT WALL
SITE LOCATIONS
MUNTA 1.
LINE 86-0194
LINE 85-0009
NORTHERN ELECTRODE
BATTERIES
EARTH
MT ARAY
10 m
HFM
INSTRUMENT
CENTER
ELECTRODE
SOUTHERN ELECTRODE
10 m

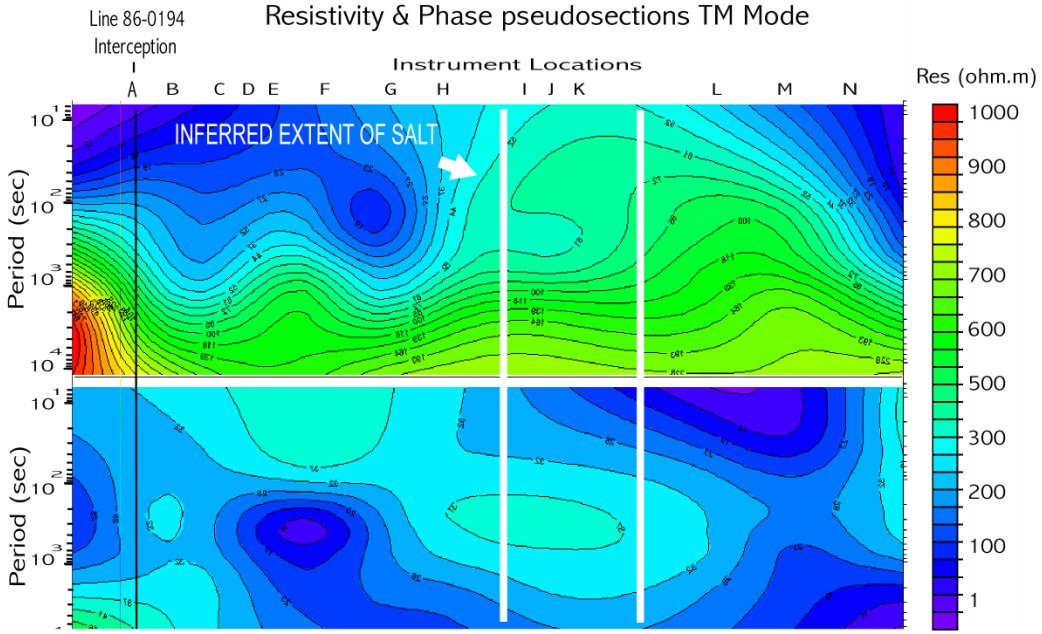
Line 86-0194
Interception
Resistivity & Phase pseudosections TM Mode
Instrument Locations
A B C D E F G H I J K L M N
Res (ohm.m)
1000
900
800
700
600
500
300
200
100
1
INFERRED EXTENT OF SALT
Period (sec)

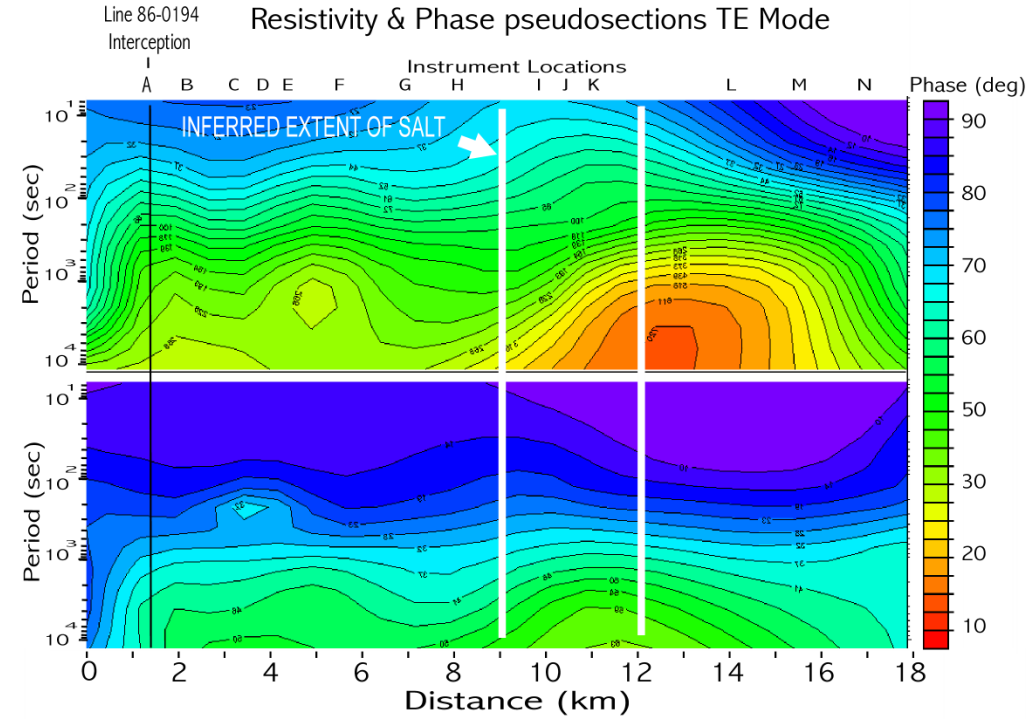
Line 86-0194
Interception
Resistivity & Phase pseudosections TE Mode
Instrument Locations
A B C D E F G H I J K L M N
Phase (deg)
90
80
70
60
50
30
20
10
INFERRED EXTENT OF SALT
Period (sec)
0 2 4 6 8 10 12 14 16 18
Distance (km)

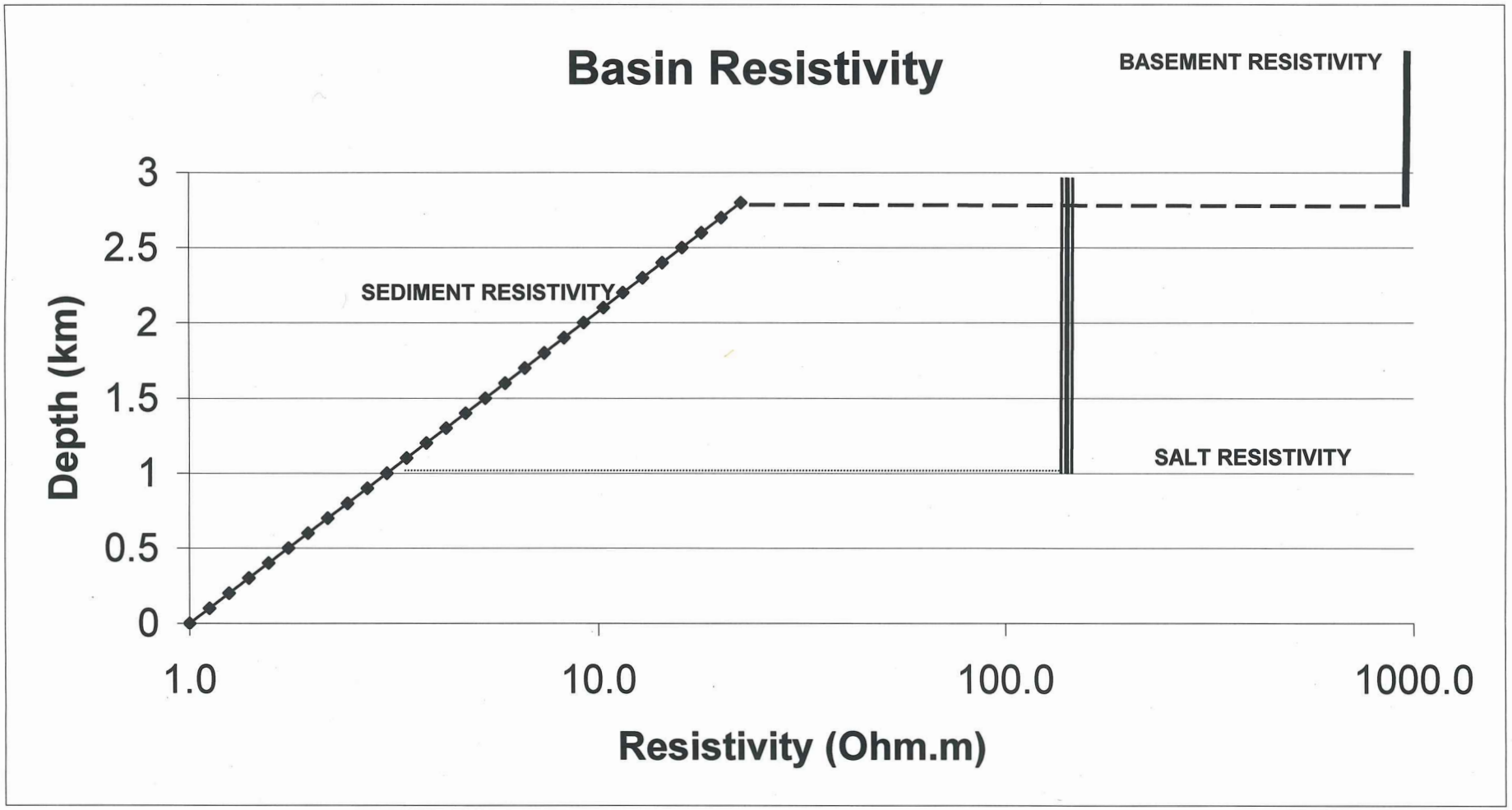
Basin Resistivity
BASEMENT RESISTIVITY
SEDIMENT RESISTIVITY
SALT RESISTIVITY
Depth (km)
3
2.5
2
1.5
1
0.5
0
1.0
10.0
100.0
1000.0
Resistivity (Ohm.m)

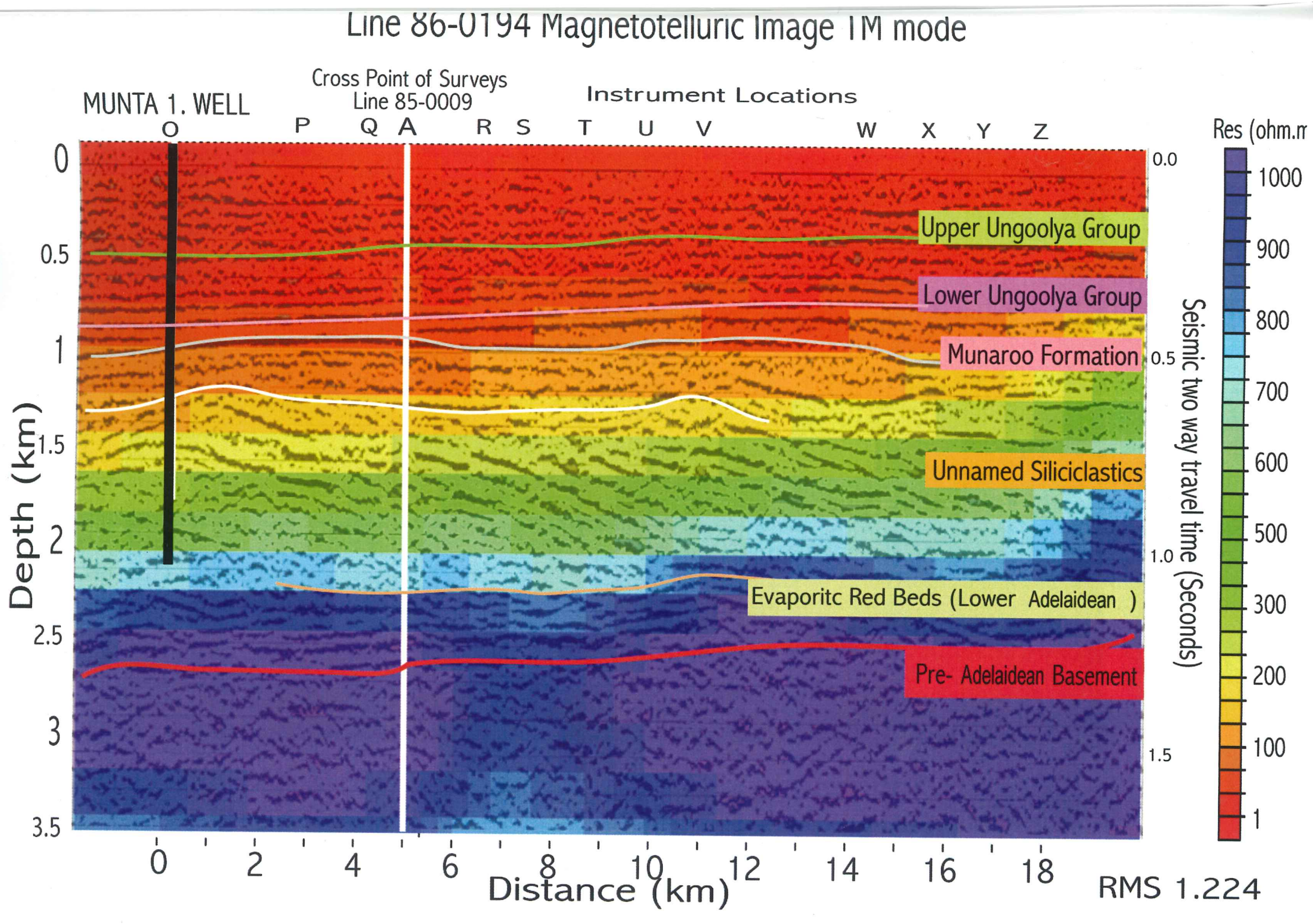
Line 86-0194 Magnetotelluric Image TM mode
MUNTA 1. WELL
Cross Point of Surveys
Line 85-0009
Instrument Locations
O
P
Q
A
R
S
T
U
V
W
X
Y
Z
Upper Ungoolya Group
Lower Ungoolya Group
Munaroo Formation
Unnamed Siliciclastics
Evaporitc Red Beds (Lower Adelaidean)
Pre- Adelaidean Basement
Depth (km)
0
0.5
1
1.5
2
2.5
3
3.5
Distance (km)
0
2
4
6
8
10
12
14
16
18
Seismic two way travel time (Seconds)
0.0
0.5
1.0
1.5
Res (ohm.m
1000
900
800
700
600
500
300
200
100
1
RMS 1.224

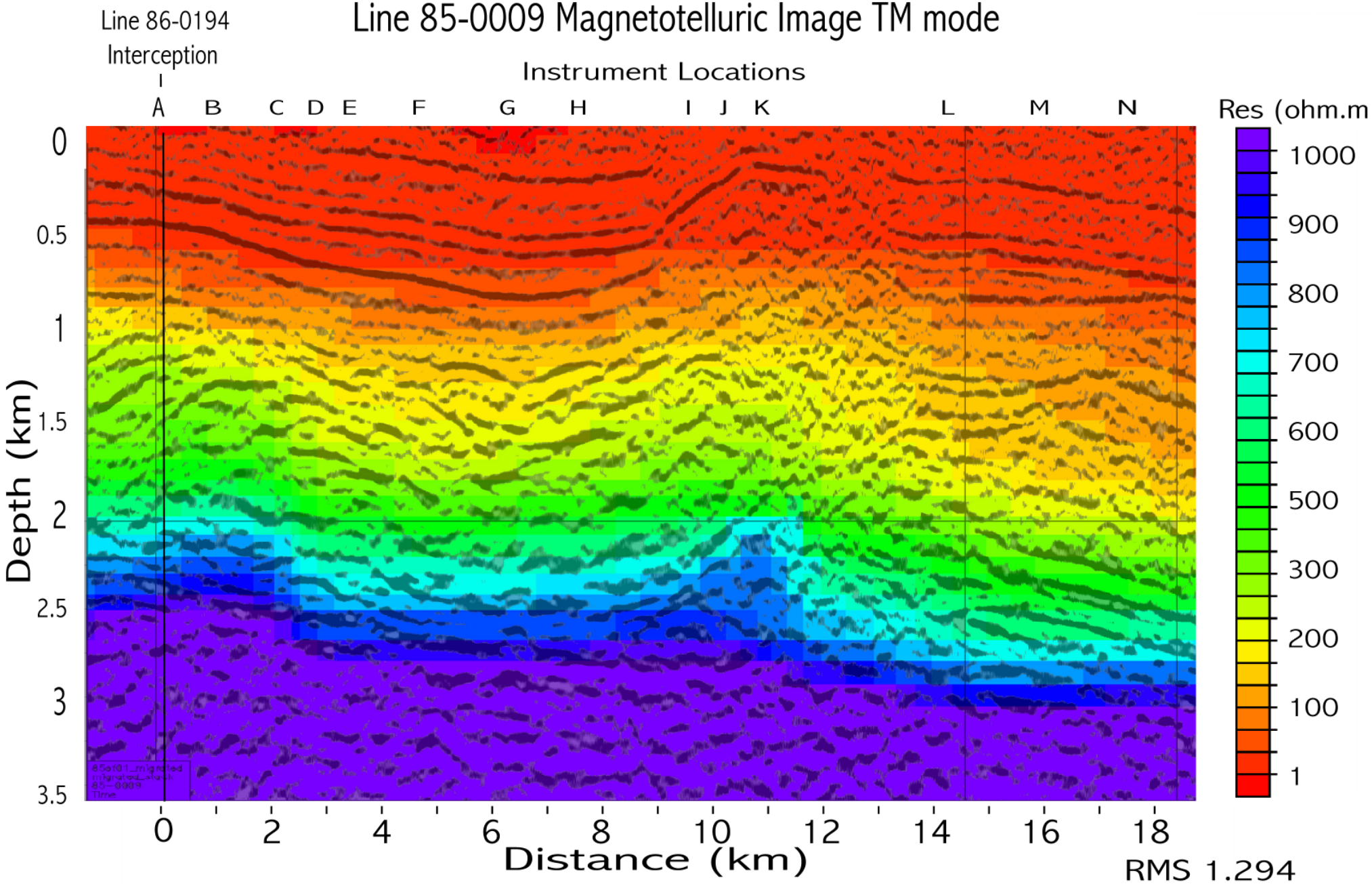
Line 85-0009 Magnetotelluric Image TM mode
Line 86-0194
Interception
Instrument Locations
A
B
C
D
E
F
G
H
I
J
K
L
M
N
Res (ohm.m
1000
900
800
700
600
500
300
200
100
1
Depth (km)
0
0.5
1
1.5
2
2.5
3
3.5
0
2
4
6
8
10
12
14
16
18
Distance (km)
RMS 1.294

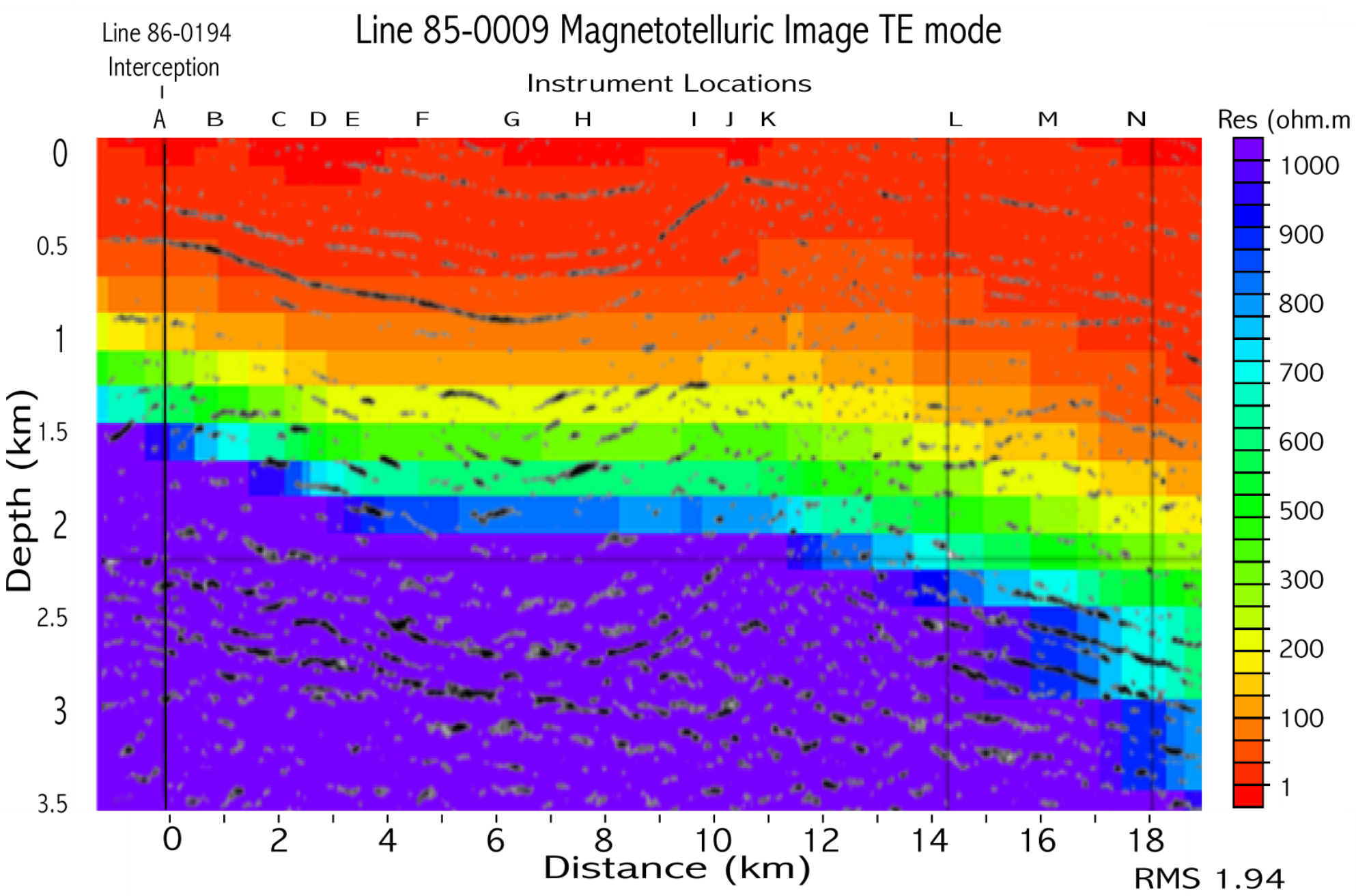
Line 85-0009 Magnetotelluric Image TE mode
Line 86-0194
Interception
Instrument Locations
A
B
C
D
E
F
G
H
I
J
K
L
M
N
Res (ohm.m
1000
900
800
700
600
500
300
200
100
1
Depth (km)
0
0.5
1
1.5
2
2.5
3
3.5
0
2
4
6
8
10
12
14
16
18
Distance (km)
RMS 1.94

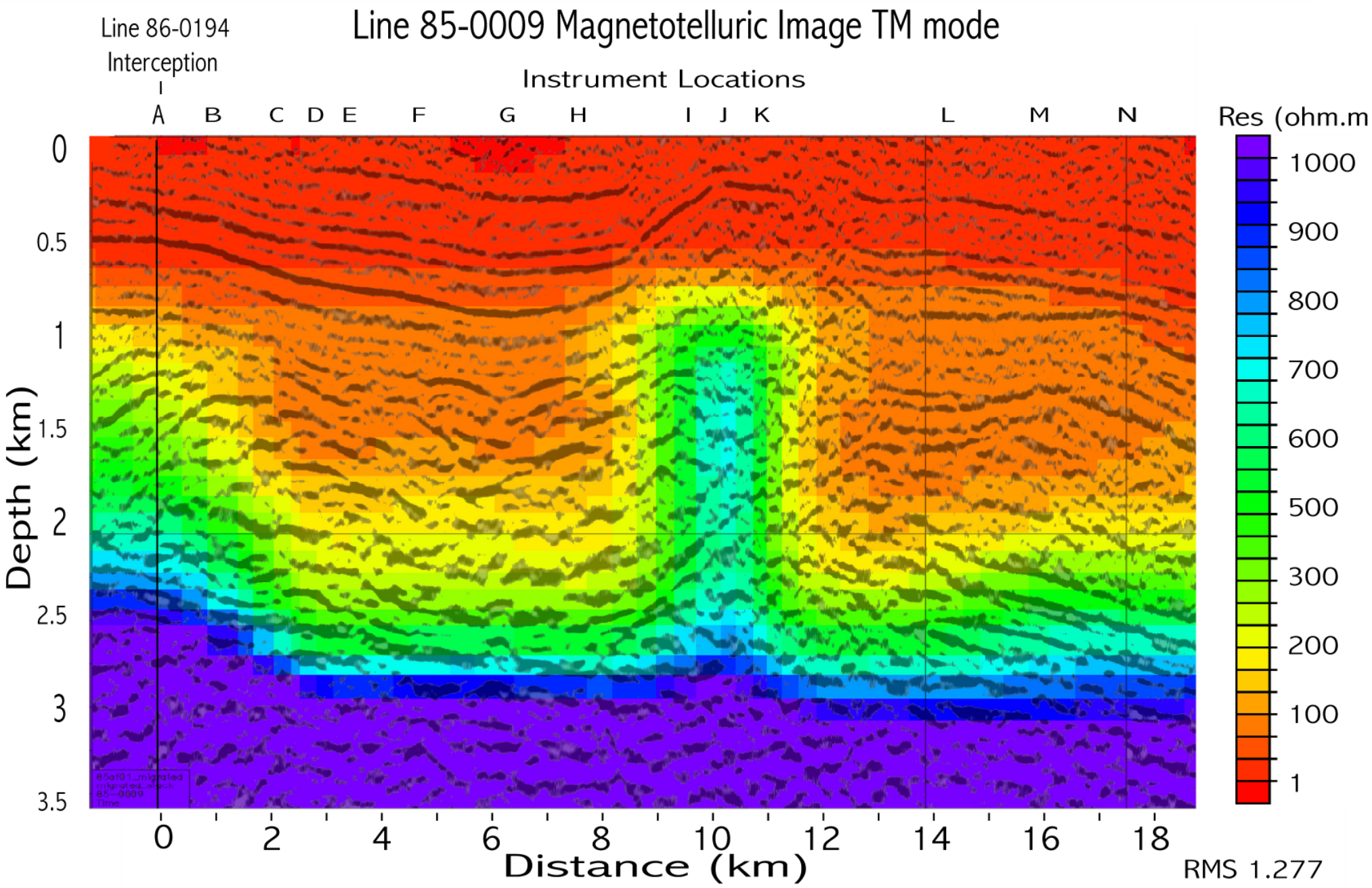
Line 85-0009 Magnetotelluric Image TM mode
Line 86-0194
Interception
Instrument Locations
A
B
C
D
E
F
G
H
I
J
K
L
M
N
Res (ohm.m
1000
900
800
700
600
500
300
200
100
1
Depth (km)
0
0.5
1
1.5
2
2.5
3
3.5
0
2
4
6
8
10
12
14
16
18
Distance (km)
RMS 1.277

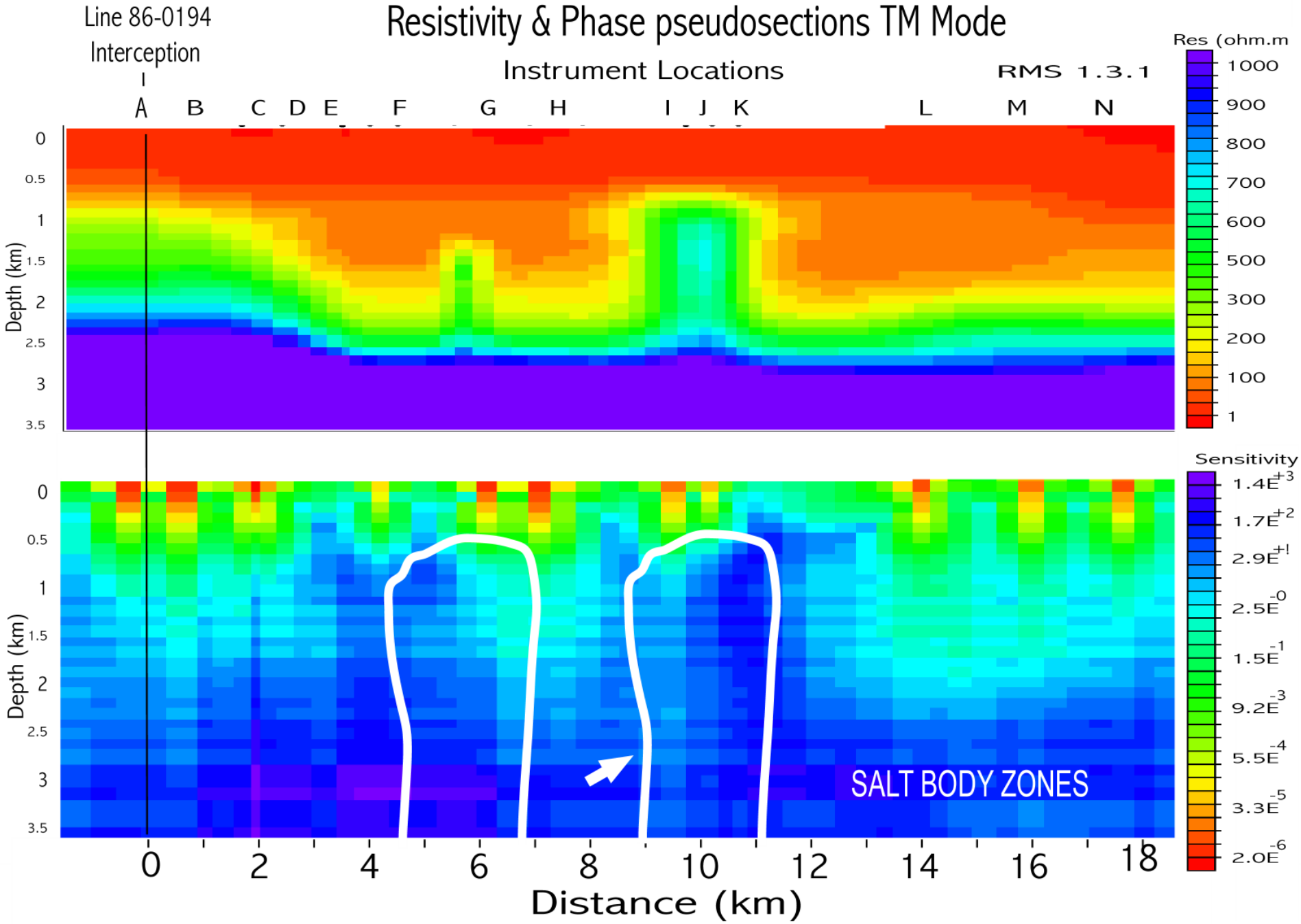
Line 86-0194
Interception
Resistivity & Phase pseudosections TM Mode
Instrument Locations
RMS 1.3.1
A B C D E F G H I J K L M N
Res (ohm.m
1000
900
800
700
600
500
300
200
100
1
Sensitivity
1.4E+3
1.7E+2
2.9E+1
2.5E-0
1.5E-1
9.2E-3
5.5E-4
3.3E-5
2.0E-6
Depth (km)
0
0.5
1
1.5
2
2.5
3
3.5
SALT BODY ZONES
0 2 4 6 8 10 12 14 16 18
Distance (km)

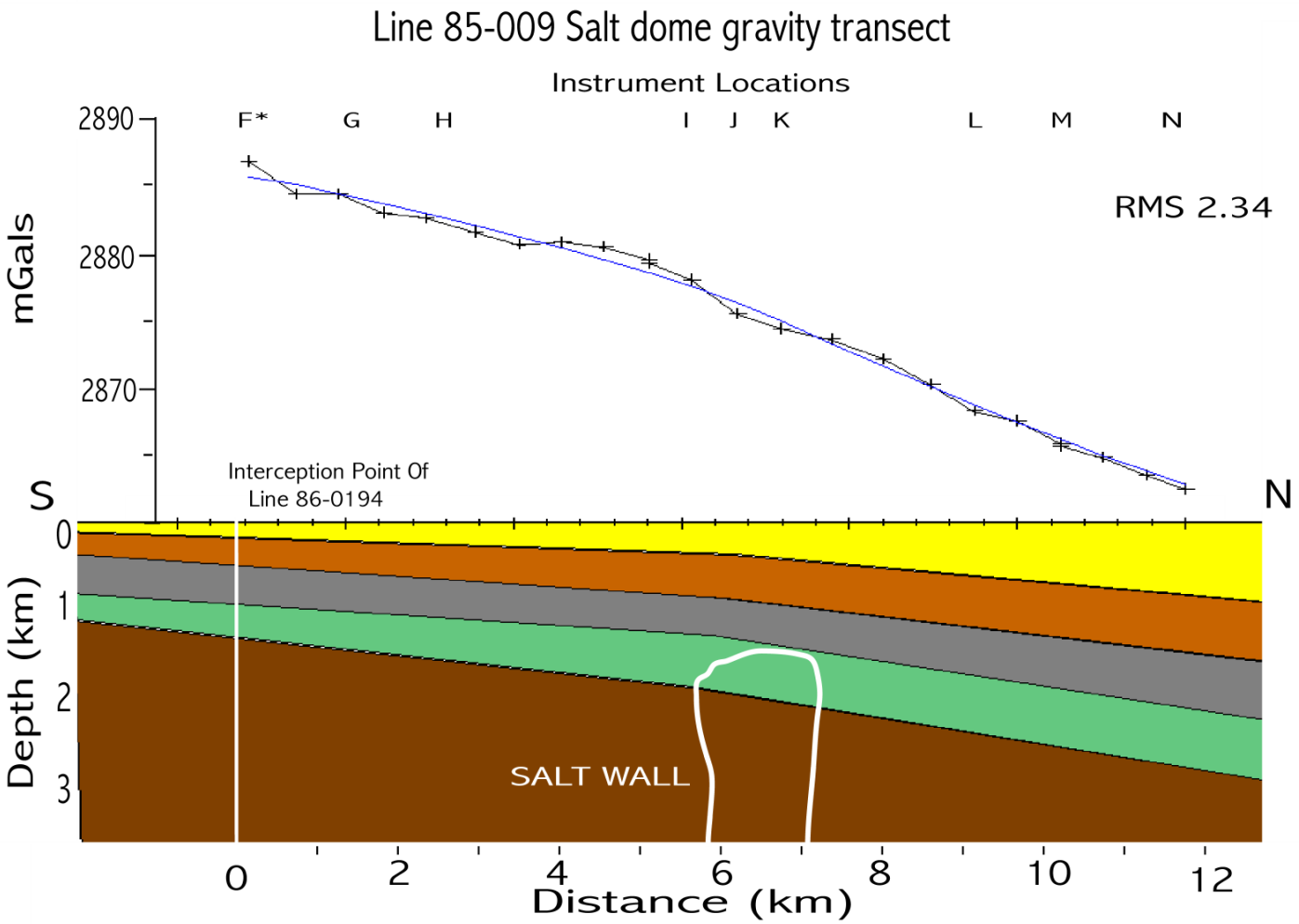
Line 85-009 Salt dome gravity transect
Instrument Locations
F*
G
H
I
J
K
L
M
N
2890
2880
2870
mGals
RMS 2.34
Interception Point Of
Line 86-0194
S
N
0
1
2
3
Depth (km)
SALT WALL
0
2
4
6
8
10
12
Distance (km)